

Palladium Nanoplate-Based IL-6 Receptor Antagonists Ameliorate Cancer-Related Anemia and Simultaneously Inhibit Cancer Progression

Jianqiang Zhu, Qingfeng Fu, Shunhao Wang, Liting Ren, Wenya Feng, Shuting Wei, Zhihong Zhang, Yong Xu, Tomas Ganz,* and Sijin Liu*



Cite This: *Nano Lett.* 2022, 22, 751–760



Read Online

ACCESS |

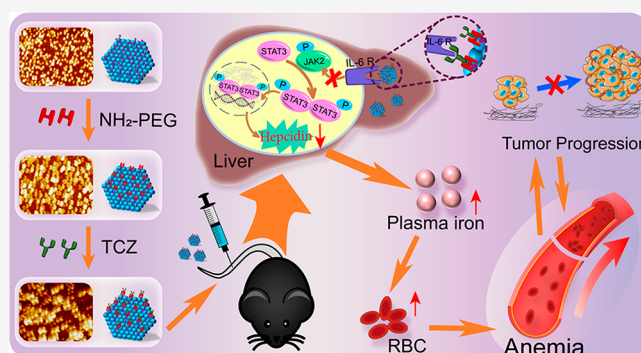
Metrics & More

Article Recommendations

Supporting Information

ABSTRACT: In recent years, targeted therapies and immunotherapeutics, along with conventional chemo- and radiotherapy, have greatly improved cancer treatments. Unfortunately, in cancer patients, anemia, either as a complication of cancer progression or as the result of cancer treatment, undermines the expected therapeutic efficacy. Here, we developed a smart nanosystem based on the palladium nanoplates (PdPLs) to deliver tocilizumab (TCZ, a widely used IL-6R antibody) to the liver for specific blockade of IL-6/IL-6R signaling to correct anemia. With chemical modifications, this nanosystem delivered a large mass of TCZ and enhanced liver delivery, inducing a marked suppression of hepcidin expression as a result of diminished IL-6 signaling. Through this mechanism, significant suppression of tumor progression was realized (at least in part) because of the corrected anemia after treatment.

KEYWORDS: cancer-related anemia, anemia of inflammation, IL-6 receptor antagonist, palladium nanoplates, tocilizumab, iron



Cancer-related anemia (CRA) is commonly found in cancer patients. Approximately, 40% of cancer patients develop anemia before treatments, and some treatments, such as radiotherapy and chemotherapy, aggravate anemia because of treatment-associated toxicities to the marrow and other organs.^{1–4} Anemia may adversely affect the physiology of many organs, and worsen outcomes, particularly in patients receiving chemotherapy or radiotherapy.⁵ Often it is difficult to determine the specific causative factor for CRA in individual cancer patients.⁶ Of note, a large portion of cancer patients with anemia exhibit persistent inflammation due to tumor-derived proinflammatory components that induce anemia of inflammation (AI).^{7–9} AI is largely attributable to the overproduction of proinflammatory cytokines, especially interleukin-6 (IL-6).¹⁰ These proinflammatory cytokines interfere with iron utilization for effective erythropoiesis⁴ and inhibit the production of endogenous erythropoietin (EPO), leading to impaired erythropoiesis.¹¹ The crosstalk between iron metabolism and erythropoiesis is closely governed by the hormone, hepcidin, which functions to limit intestinal iron absorption and iron egress from macrophages by binding to the iron exporter, ferroportin.¹² Hepcidin levels are subject to regulation by a number of factors and conditions, and inflammation is a particularly strong driving force in promoting hepcidin expression.¹³ IL-6 plays a key role in eliciting hepcidin transcription through JAK/STAT3 signaling, causing iron

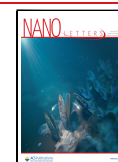
retention in macrophages and decreasing dietary iron absorption, consequently reducing the iron supply for erythropoiesis.¹⁴ Blocking IL-6-mediated inflammatory signaling that stimulates hepcidin production should be an effective strategy against anemia.

To date, multiple effective IL-6 or IL-6 receptor (IL-6R) antagonists have been developed to block IL-6 signaling to treat various diseases, such as arthritis and autoimmune diseases. Tocilizumab (TCZ) is a widely used IL-6R antagonist for the treatment of rheumatoid arthritis through the blockade of IL-6/IL-6R cascade signaling,^{15,16} which binds to both soluble IL-6R (sIL-6R) and membrane IL-6R (mIL-6R) in a dose-dependent manner.¹⁷ Encouragingly, a previous study suggested that TCZ could correct anemia in monkey arthritis by inhibiting hepcidin production.¹⁸ Considering that hepcidin is exclusively synthesized and secreted by hepatocytes in the liver, we hypothesized that selective blockade of IL-6R signaling in hepatocytes would

Received: November 6, 2021

Revised: January 7, 2022

Published: January 14, 2022



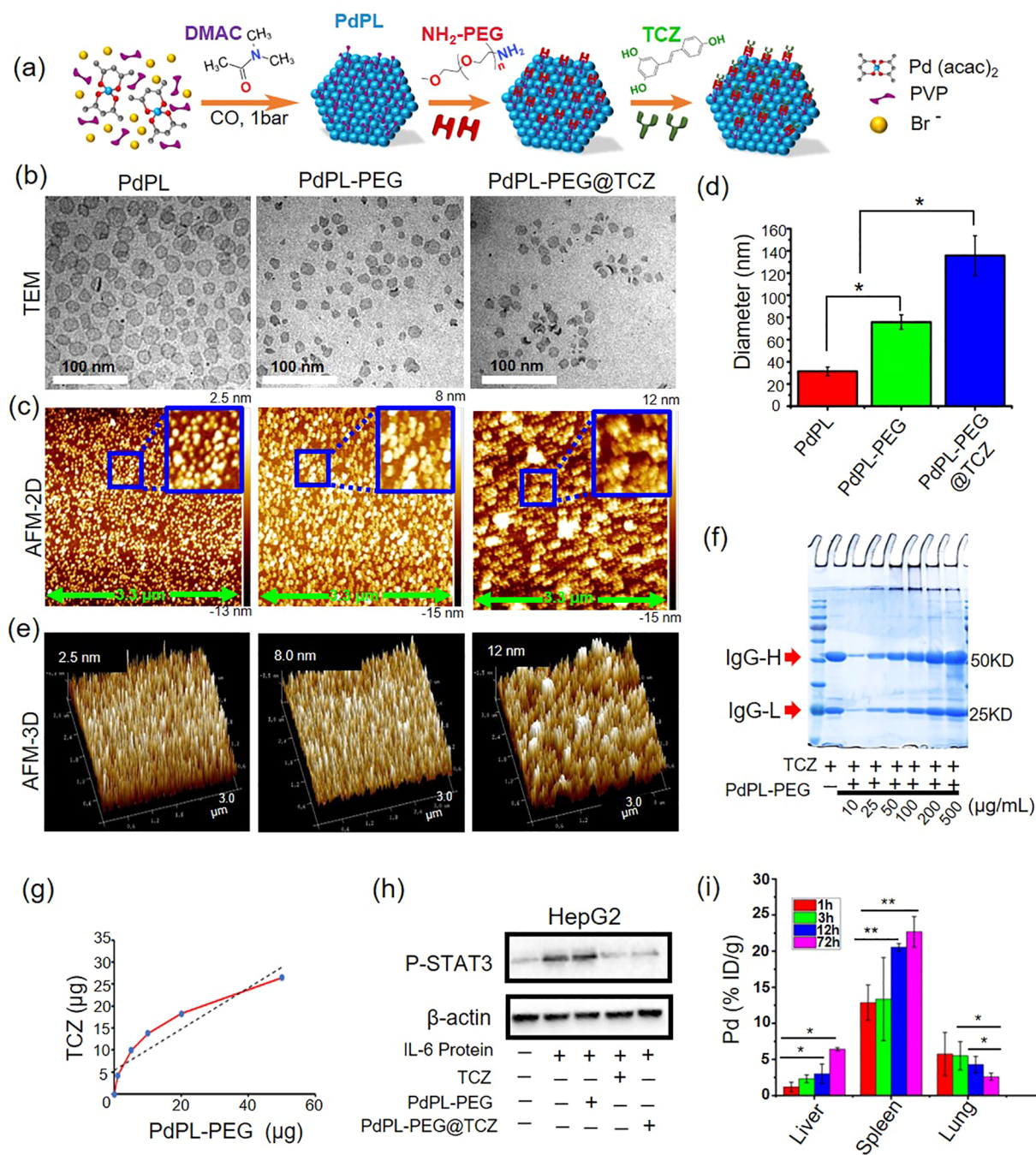


Figure 1. Physicochemical characterization of synthesized PdPL complexes and the in vitro and in vivo determination of PdPL nanomedicines. (a) Schematic depicting the modification of PdPLs with NH_2 -PEG and the following loading of TCZ. (b–e) Representative TEM images (b), AFM 2D images (c), measured diameter of these materials based on the AFM 2D images (d), and AFM 3D images of the surface topography (e) for pristine PdPLs, PdPL-PEG, and PdPL-PEG@TCZ. (Blue solid wireframes in panel c indicate enlarged AFM images. Luminance scale at the right side of each image in panel c denotes the height of nanomaterials). (f) Coomassie blue staining of TCZ (at $100 \mu\text{g}/\text{mL}$) that was lodged on PdPL-PEG at different concentrations. (g) Loading capacity of TCZ on the surface of PdPL-PEG. (h) Blocking efficacy of PdPL-PEG@TCZ on the IL-6-STAT3 signaling, as reflected by the levels of phosphorylated STAT3 (P-STAT3). (i) Mass of Pd in heart, liver, spleen, lung, kidney, and bone marrow at 1, 3, 12, and 72 h post intravenous administration of the nanomaterials, as detected by ICP-MS ($n = 5$). *, $P < 0.05$; **, $P < 0.001$.

diminish hepatic hepcidin expression without affecting the physiological function of IL-6R in other tissues and organs.

To this end, we designed a new nanoparticle formulation, hexagonal palladium nanoplate (PdPL)-based nanoagents with NH_2 -PEG coating, which offers an ample platform for molecule loading. These PdPL nanoagents were further loaded with an effectively amount of TCZ on the particle surface for the

purpose of selective targeting IL-6R in the liver. Together, our

results reveal the potential of TCZ-based nanomedicines in

treating CRA and inducing useful anticancer effects.

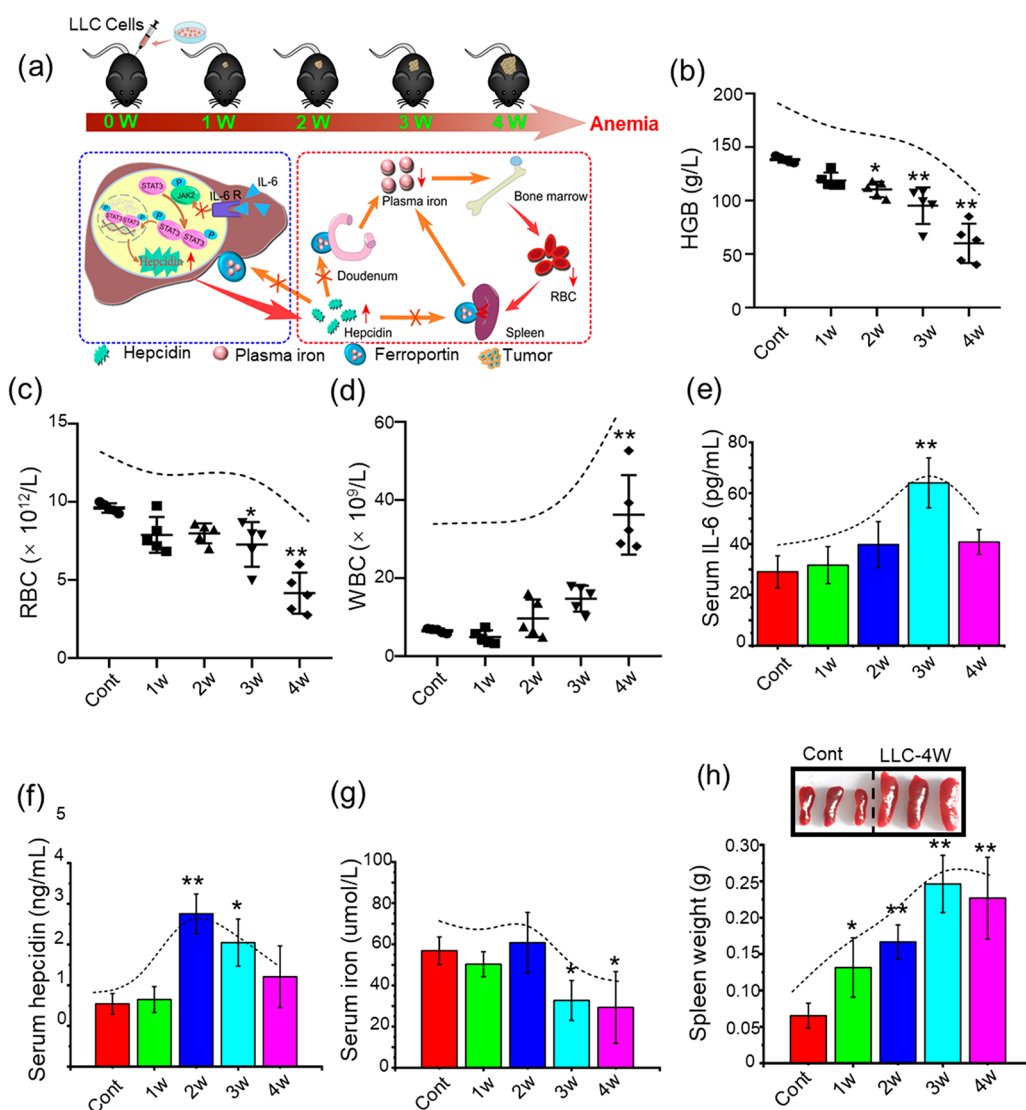


Figure 2. Establishment of the CRA mouse model. (a) Schematic diagram illustrating the experimental design for the establishment of mouse model for anemia of cancer, with lower panel showing iron recycling and modulation by the liver through the IL-6/STAT3/hepcidin signaling. (b–h) Compared to the control, mice injected with LLC cells manifested reduced levels of hemoglobin content (b) and RBC count (c) starting from 2 weeks, and otherwise elevated inflammation as characterized by increased WBC count (d) and serum IL-6 concentrations (e). These mice revealed increased hepcidin in serum (f). In the meantime, the serum iron concentrations were diminished in these tumor-bearing mice relative to the control mice (g). (h) The weight of spleens from mice after LLC cell implantation for 1, 2, 3, and 4 weeks are shown within histogram, and the representative images of spleens from mice after 4 weeks of LLC cell implantation are shown in contrast to spleens from the control mice in the upper panel. *, $P < 0.05$; **, $P < 0.001$, compared to the control group ($n = 5$).

■ FABRICATION OF TCZ NANOCOMPLEXES BASED ON PDPLS FOR SELECTIVE LIVER TARGETING

First, we aimed to fabricate TCZ nanoagents to enhance their efficacy in targeting liver cells. Although TCZ has been widely used to treat rheumatoid arthritis in clinical practice, it is systemically distributed, exposing organs and tissue throughout the body to the effects of the drug. For the purpose of hepatic hepcidin regulation and the treatment of anemia of inflammation, selective liver targeting of TCZ is desirable. As most nanomaterials localize in the liver, where the small particles are ingested by the reticuloendothelial macrophages of this organ,^{19–21} we utilized this selectivity to load particles with TCZ for liver delivery.

The rapid development of nanotechnologies offers unprecedented opportunities and advantages in designing new strategies for therapeutics and diagnostics. Our recent studies demon-

strated that palladium (Pd)-based nanomaterials (such as Pd nanoplates and PdPLs) are outstanding nanoagents in cancer therapeutics due to their desirable physicochemical properties, such as biocompatibility/cytocompatibility, drug loading capacity, and favorable photothermal and photoacoustic properties.^{22,23} Here, we adopted PdPLs as a delivery vehicle to transport TCZ to the liver, as delineated in Figure 1a. To increase the loading capacity, the surface of PdPLs was chemically modified with $\text{NH}_2\text{-PEG}$, as demonstrated previously.²⁴ After TCZ attachment, the nanocomplexes were thoroughly characterized. As shown in Figure 1b, in contrast to the uniform lamellar plate-like 2D structure for the intact PdPLs, detectable morphological alterations were observed in PdPL-PEG, especially after TCZ loading, as evidenced by the thickening of the plate and the curling around the edge area. In agreement with this observation, the 2D- and 3D-AFM

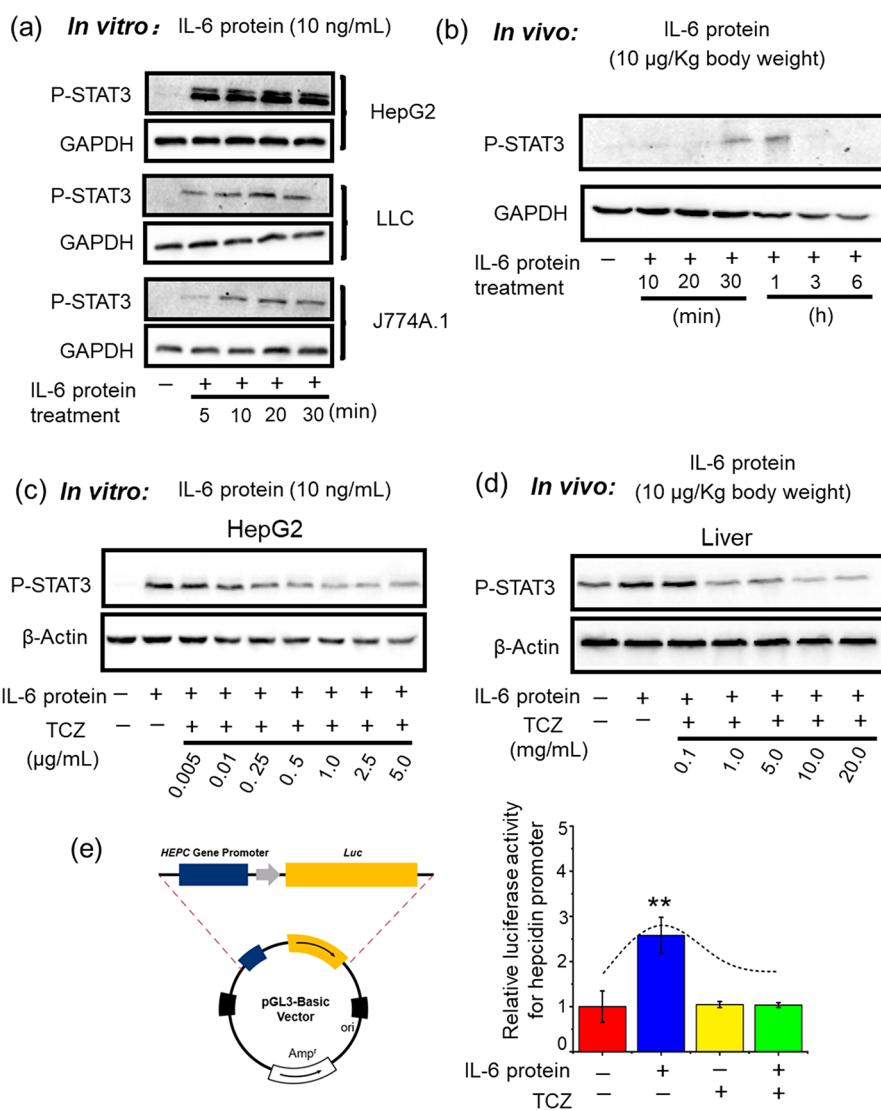


Figure 3. Efficacy of TCZ in suppressing hepcidin through the IL-6/STAT3 signaling. (a, b) The levels of phosphorylated STAT-3 (P-STAT3) in HepG2 cells, LLC cells and J774A.1 cells upon recombinant IL-6 treatment for different time (a) and in the liver from mice upon IL-6 administration (b). (c, d) Levels of P-STAT3 in HepG2 cells (c) and in mice (d) upon concomitant treatment of IL-6 and TCZ. (e) Dual-luciferase reporter assay dependent on the hepcidin promoter was used to determine the blocking effects of TCZ pretreatment on hepcidin expression in HepG2 cells. **, $P < 0.001$ compared to the untreated control ($n = 5$).

analyses corroborated these morphological changes, as the NH_2 -PEG modification altered the height, size, and surface morphology of nanoparticles and the morphology and structure changed further after TCZ loading, as shown in Figure 1c–e. Specifically, the diameter measurement showed a gradual increase from 31.37 to 75.72 and 135.72 nm for PdPLs, PdPL-PEG, and PdPL-PEG@TCZ (Figure 1d, $P < 0.05$), indicating the formation of nanocomplexes on the surface of PdPLs and the overall expansion of the material size post TCZ loading.

Next, the amount of TCZ loading on the PdPL-PEG surface was assayed by Coomassie brilliant blue staining of the SDS-PAGE gel. As shown in Figure 1f, TCZ was effectively loaded onto the PdPL-PEG surface even at a very low concentration, that is, 10 µg/mL, and more TCZ could be added onto PdPL-PEG with increased concentrations, showing a dose-dependence evidenced by the increasing staining of the IgG heavy and light chains, IgG-H and IgG-L. The mass ratio of TCZ and PdPLs was calculated to be approximately 1:2 (Figure 1g). Next,

we compared the potency of PdPL-PEG@TCZ complexes on IL-6R/STAT3 signaling in comparison to an equal amount of free TCZ. As shown in Figure 1h, free TCZ and PdPL-PEG@TCZ complexes comparably suppressed the phosphorylation of STAT3 in HepG2 cells, compared to that in cells treated with IL-6 only. Of note, PdPL-PEG itself did not alter the level of P-STAT3. Furthermore, we assessed the selectivity of liver targeting of the PdPL-PEG@TCZ complexes. The tissue distribution of Pd over the time course was determined by ICP-MS analysis following intravenous injection of these materials. Consistent with most nanomaterials,^{25,26} the liver, spleen, and lung are the most prominent sites for material accumulation (Figure 1i). Intriguingly, PdPLs gradually accumulated in the liver and spleen from 1 to 3, 12, and 72 h ($P < 0.05$), while there was a continuous decline in material accumulation in the lung (Figure 1i, $P < 0.05$), indicative of the redistribution of PdPL-PEG@TCZ nanomaterials from the lung to the liver and spleen. The increasing accumulation of PdPLs in the liver may be ascribed to a few mechanisms, including differential uptake

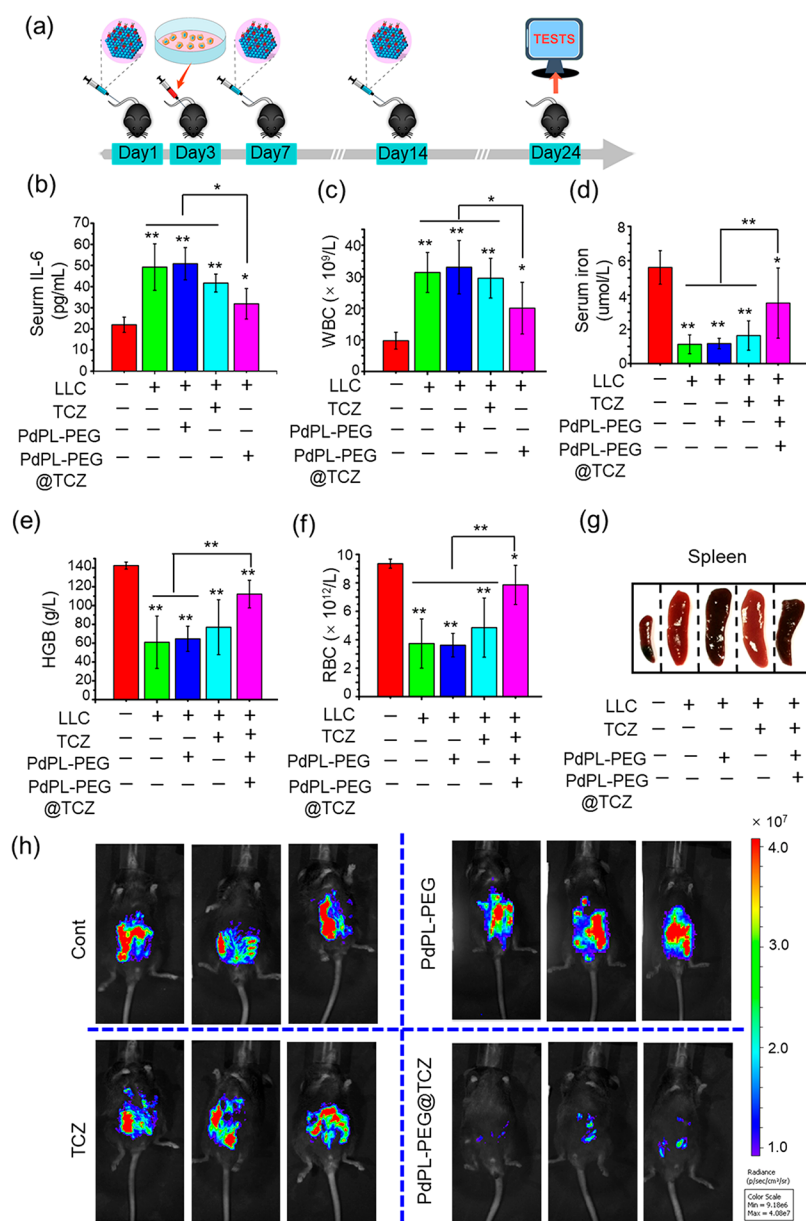


Figure 4. Therapeutic effects of PdPL-PEG@TCZ in the CRA model derived from LLC tumor cells. (a) Schematic diagram delineating the experimental design, where the CRA mouse model was established through intraperitoneal injection of LLC cells, followed by PBS, PdPLs, TCZ, or PdPL-PEG@TCZ administration (the dose of TCZ was 5 mg/kg body weight, and PdPL-PEG@TCZ carried the same mass of TCZ relative to the free TCZ control group). At the end of experiments, (b) serum IL-6 levels, (c) WBC counts, (d) serum iron levels, (e) HGB levels, (f) RBC counts, and (g) spleen changes were determined. (h) Tumor growth was assessed through the bioluminescence in indicating the mass of LLC cells. Bioluminescent images were acquired on day 21 in mice post intraperitoneal injection of LLC cells with or without treatments. *, $P < 0.05$; **, $P < 0.001$, relative to untreated control or between indicated groups ($n = 5$).

kinetics by the reticuloendothelial system in the liver, secondary distribution from other organs into the liver, and excretion from lymphatic tissue into the liver.^{27–30} Nevertheless, this represents a preferential feature for our PdPLs to target the liver. Additionally, our nanomaterials manifested complete biosafety and biocompatibility in animals, as reflected by normal tissue histology and inflammatory indicators (Figures S1 and 2).

ESTABLISHMENT OF A CRA MOUSE MODEL TO TEST TCZ NANOAGENTS

We, first, established a CRA mouse model through implantation of LLC cancer cells via the intraperitoneal injection route, as depicted in Figure 2a. The hemoglobin (HGB) content and red

blood cell (RBC) count gradually decreased from 1 to 4 weeks postimplantation of LLC cells relative to that in the untreated control group ($P < 0.05$ at weeks 2, 3, and 4). After 4 weeks, the HGB content and RBC count were reduced by almost 60% relative to those in the control group (Figure 2b and c, $P < 0.001$). The mice showed systemic inflammation, as indicated by the elevated white blood cell (WBC) count and serum IL-6 concentration compared to those in the untreated control group (Figure 2d and e, $P < 0.001$), and their serum hepcidin level was significantly induced by more than 2-fold at 2 weeks after LLC cell injection relative to the untreated control (Figure 2f, $P < 0.001$). By 4 weeks, both IL-6 and hepcidin levels declined to basal levels (Figure 2e and f). As a consequence of hepcidin

induction, systemic iron was redistributed. As shown in Figure 1g and Figure S3a, the serum iron concentration was reduced by approximately 50% by 3 weeks, and splenic iron increased, consistent with iron sequestration in the spleen that limited the iron supply for erythropoiesis. Similar to other studies,³¹ hepatic iron content changed little (Figure S3b). Marked splenomegaly developed in the CRA mice (Figure S3c and 1h), indicative of extramedullary erythropoiesis in the spleen.

TCZ BLOCKS IL-6-MEDIATED HEPCIDIN INDUCTION

We next verified the efficacy of TCZ in blocking IL-6R/STAT3 signaling. We used human IL-6 (hIL-6) recombinant protein to trigger the activation of IL-6R/STAT3 signaling in 3 different cell lines, HepG2, LLC, and J774A.1, at a concentration of 10 ng/mL. P-STAT3, a marker for the activation of IL-6R/STAT3 signaling,³² was thereafter assessed at different time points. As shown in Figure 3a, the level of P-STAT3 was rapidly induced in these 3 types of cells after IL-6 addition, indicative of the activation of IL-6R/STAT3 signaling. After hIL-6 administration to mice at 10 μ g/kg body weight, the P-STAT3 level was increased as soon as 30–60 min after hIL-6 administration (Figure 3b), but the STAT3 level returned to the baseline by 3 h, in agreement with previous observations suggestive of feedback repression of the inflammatory responses.³³

Moreover, TCZ was used to block IL-6R/STAT3 signaling *in vitro* and *in vivo*. As shown in Figure 3c, pretreatment with TCZ at various concentrations considerably repressed the phosphorylation of STAT3 in HepG2 cells in response to hIL-6 in a dose-dependent manner, as clearly reflected by the reduced levels of P-STAT3. Additionally, after hIL-6 administration in mice, TCZ pretreatment suppressed STAT3 phosphorylation in a dose-dependent manner; however, TCZ pretreatment did not completely block IL-6/STAT3 signaling even at higher doses (Figure 3d). These findings thus indicated a reasonable efficacy of TCZ in blocking murine IL-6R; a limitation still exists, likely due to the discrepancy in molecular structure between humans and mice.³⁴

Since the expression of hepcidin is directly driven by the IL-6R/STAT3 signaling,³⁵ a hepcidin promoter reporter construct, developed previously in our laboratory,³⁶ was employed to assay the ability of TCZ to inhibit IL-6 induced hepcidin expression (Figure 3e). Consistent with previous findings,⁷ IL-6 induced hepcidin promoter activity by 2.6 fold, as evidenced by the increase in luciferase bioluminescence (Figure 3e, $P < 0.001$). However, this increase was completely reversed by TCZ relative to the untreated control (Figure 3e, $P < 0.001$). Together, these data confirmed that TCZ effectively inhibited hepcidin expression by blocking the IL-6/STAT3 signaling pathway.

PDPL-PEG@TCZ POTENTLY AMELIORATED ANEMIA AND INHIBITED TUMOR GROWTH IN THE LLC MODEL

We, subsequently, evaluated the effects of PdPL-PEG@TCZ on anemia, inflammation, and tumor growth, as illustrated in Figure 4a. PdPL-PEG@TCZ decreased serum IL-6 levels more effectively than free TCZ at the same concentration (by 35% vs 15%, $P < 0.05$); the levels in untreated mice were used as the control (Figure 4b, $P < 0.05$). Additionally, PdPL-PEG@TCZ ameliorated leukocytosis more effectively than free TCZ (Figure 4c, $P < 0.05$). PdPL-PEG@TCZ administration increased the serum iron concentration, HGB content and RBC count to

nearly normal values in wild-type mice (Figure 4d–f, $P < 0.05$). In general, PdPL-PEG@TCZ was more potent than free TCZ at inducing these effects (Figure 4d–f, $P < 0.001$), likely because PdPL-PEG nanocarriers facilitate more specific delivery of TCZ to the liver. In support of these data, splenomegaly in PdPL-PEG@TCZ-treated mice was greatly improved, as demonstrated by a 32% reduction in spleen weight relative to that in untreated mice (Figures S4 and 4g, $P < 0.05$). Additionally, histological examination confirmed the substantial improvement of extramedullary erythropoiesis in the spleen in mice upon PdPL-PEG@TCZ but not in other groups (Figure S5). These improvements were greater than those seen with free TCZ, confirming the greater potency of PdPL-PEG@TCZ than free TCZ in correcting CRA. Strikingly, tumor growth was also constrained. As shown in Figure 4h, 3 weeks after treatment, mice treated with PdPL-PEG@TCZ had nearly no tumor bioluminescence signal in the abdominal cavity, while those with free TCZ treatment showed comparable bioluminescence to that in untreated mice. The nanocarrier PdPL-PEG alone did not inhibit inflammation or alleviate anemia or tumor progression. These results together indicated that PdPL-PEG@TCZ potentially ameliorates anemia and simultaneously represses tumor growth.

PDPL-PEG@TCZ PER SE REVEALED AN INHIBITORY EFFECT ON TUMOR GROWTH OF 4T1 CELLS

To clarify the suppressive effects of PdPL-PEG@TCZ on LLC cell-derived tumor growth, we intended to differentiate the direct repression of PdPL-PEG@TCZ on cancer cell growth from the indirect effect of correcting anemia. For this purpose, we addressed this issue using different *in vitro* and *in vivo* models. First, as shown in Figure S6, hIL-6 exhibited a slight enhancing effect on LLC and 4T1 cell proliferation at 20 ng/mL *in vitro* (Figure S6a and b), consistent with previous studies,^{32,37} but TCZ alone elicited little effect on cell proliferation (Figure S6c and d). Nonetheless, the slight hIL-6-stimulated increase in cell growth was diminished by the addition of TCZ in both LLCs and 4T1 cells (Figure S6e and f, $P < 0.05$). Similar observations were also found in A498 and EJ cells (Figure S6g and h, $P < 0.05$). These results revealed a mild stimulatory effect of hIL-6 on cancer cell proliferation, and TCZ could effectively reverse this effect *in vitro* by blocking IL-6 signaling.

Furthermore, we established a mouse model with marked inflammation, including IL-6 induction, but without anemia. As described in our previous studies, we established a murine breast cancer model through orthotopic injection of 4T1 cells.^{38–40} As shown in Figure S7a and b, gradually elevated inflammation was induced in mice responding to 4T1 tumor progression, as evidenced by remarkable increases in WBC count and serum IL-6 concentrations over the time course from 1 to 4 weeks ($P < 0.05$). However, no anemia was found in these mice harboring 4T1 tumors, as characterized by little change in HGB content and RBC count over time (Figure S7c and d). These data suggest an ideal cancer model with inflammation but without anemia, although the detailed mechanisms are not understood and warrant future investigation. Nevertheless, this model could be used to recognize the direct effect of PdPL-PEG@TCZ nanocomplexes on tumor growth by excluding the indirect effect dependent on the amelioration of anemia.

Next, to determine the therapeutic effect of PdPL-PEG@TCZ on 4T1 tumor progression, we adopted a regimen similar to that for the LLC model (Figure 4a), as illustrated in Figure

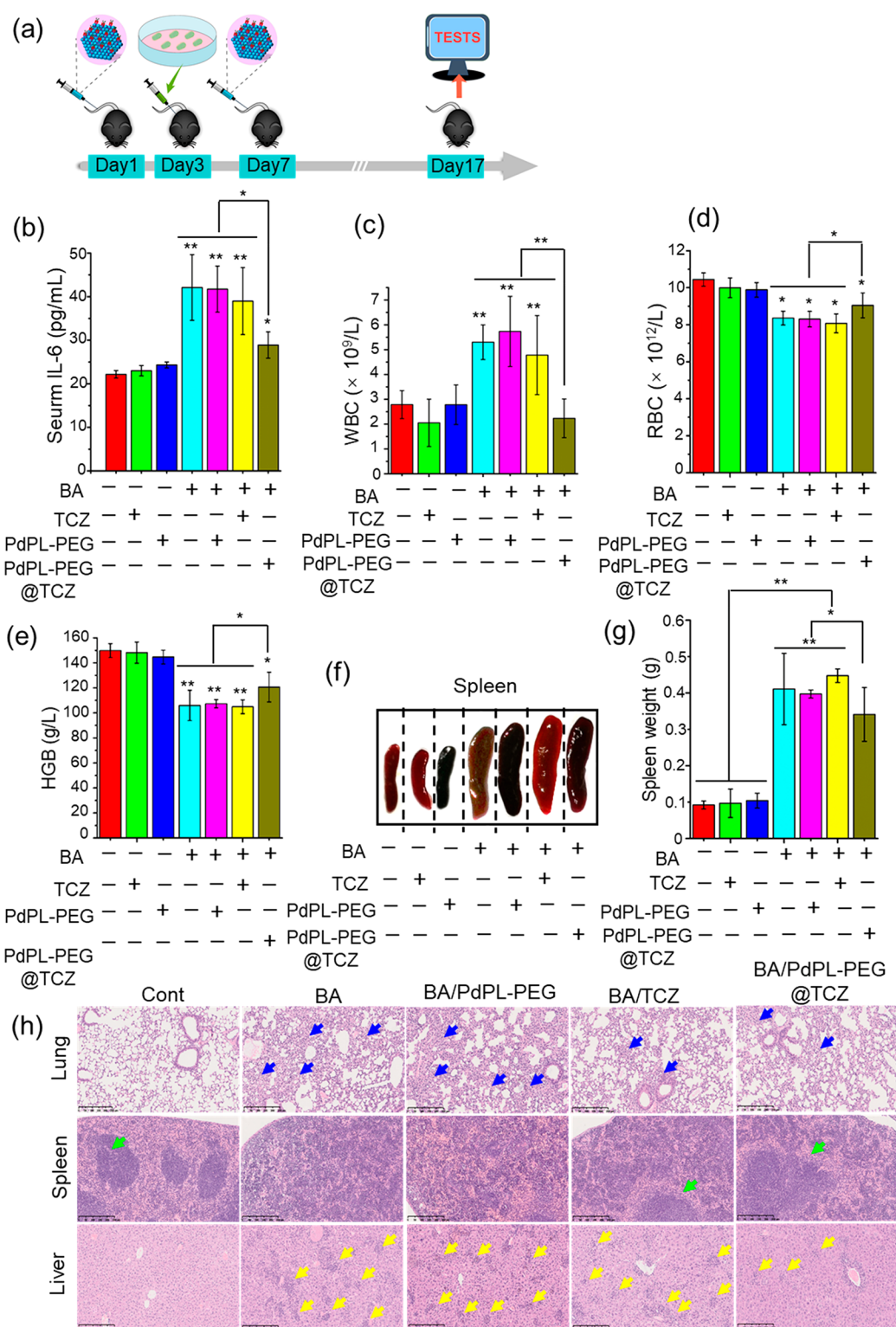


Figure 5. Therapeutic efficacy of PdPL-PEG@TCZ in the AI model induced by BA. (a) Schematic diagram showing the experimental design, where the mouse model of BA-induced anemia was developed. After treatments, (b) serum IL-6 levels, (c) WBC counts, (d) RBC counts, (e) HGB levels, and (f–g) spleen changes were examined. Meanwhile, (h) histological examination was performed in lung, spleen, and liver from different groups. Blue arrows indicate the accumulation of inflammatory cells in the lung. Green arrows denote the intact structure of white pulps in the spleen. Yellow arrows point at the infiltration of inflammatory cells in the liver. The administration dose of TCZ was 5 mg/kg body weight, whereas PdPL-PEG@TCZ carried the same mass of TCZ relative to the free TCZ control. The injection volume was 100 μ L per mouse. *, $P < 0.05$; **, $P < 0.001$, relative to untreated control or between indicated groups ($n = 5$).

S8a. PdPL-PEG, TCZ, and PdPL-PEG@TCZ administration did not influence the body weight of all mice, compared to untreated control mice (Figure S8b), reflective of great

biocompatibility of these materials. Importantly, as shown in Figure S8c–e, 4T1 tumor progression was controlled in mice upon PdPL-PEG@TCZ administration, albeit much weaker

than the suppressive effect observed in the LLC model (Figure 4). Specifically, the final average tumor weight was reduced by 38.41% in PdPL-PEG@TCZ-treated mice relative to the untreated control (Figure S8e, $P < 0.05$). In contrast, treatment with PdPL-PEG or TCZ had little impact on 4T1 tumor progression (Figure S8c–e), stressing the necessity of TCZ assembly and targeting to tumors using the PdPL-PEG nanocomplex. These findings therefore uncover a direct inhibitory effect of PdPL-PEG@TCZ on 4T1 tumor growth through blocking the IL-6 signaling, albeit much milder than the inhibition on LLC tumor growth. Together, our experiments in the nonanemic cancer model (Figures S7 and S8) indicate that the anticancer effect of nanoformulated TCZ is not solely mediated by the reversal of anemia. Moreover, we also provided evidence that TCZ could directly inhibit the IL-6-stimulated growth of various tumor cell lines (Figure S6). To this end, these findings support a robust capability of PdPL-PEG@TCZ to suppress tumor progression through both direct and indirect mechanisms. Nevertheless, complex direct and indirect effects may coexist and be intertwined, as is common with anticytokine therapies.⁴¹

■ PDPL-PEG@TCZ CONSIDERABLY ALLEVIATED AI INDUCED BY HEAT-KILLED *BRUCELLA ABORTUS* (BA)

To corroborate the benefits of PdPL-PEG@TCZ in correcting anemia due to inflammation, as an extension, we further employed an AI mouse model induced by heat-killed BA cells, as reported.⁴² Similar to the strategy used above for the CRA model, PdPL-PEG@TCZ was administered and compared to free TCZ at the same concentration before and after BA infection, as illustrated by the diagram in Figure 5a. As shown in Figure 5b–h, the AI model caused by intraperitoneal injection of BA was characterized by elevated systemic and tissue inflammation, reduced RBC count, and extramedullary erythropoiesis. Free TCZ manifested rather limited potency in correcting AI, as evidenced by slight changes in these factors in comparison to untreated mice (Figure 5b–h). However, PdPL-PEG@TCZ significantly improved these AI indexes. Specifically, PdPL-PEG@TCZ administration decreased systemic and local inflammation, as the serum IL-6 level and WBC count nearly reached baseline values seen in the wild-type mice, and inflammatory cell infiltration in the liver and lung was greatly diminished (Figure 5b, c, and h, $P < 0.05$). Moreover, PdPL-PEG@TCZ increased the RBC count and HGB level, and ameliorated splenomegaly (Figure 5d–h, $P < 0.05$). Similar to the results observed in the CRA model, PdPL-PEG alone was inactive in this model. Together, these results suggested that both cancer-related anemia and the anemia induced by BA share the involvement of IL-6 and hepcidin in the pathogenesis of the anemia and further supported the enhanced capability of PdPL-PEG@TCZ to alleviate AI in a bacteria-induced inflammatory model.

To date, the applications of TCZ in different species other than humans are still debated. Some studies reported a reliable effect of TCZ in murine models,^{7,43–45} whereas others did not.^{34,46} Our data demonstrated notable but not full efficacy in blocking IL-6/IL-6R signaling in these mouse models. This divergence from the expected results could be ascribed to different cell lines, genetic backgrounds, experimental conditions, and local and systemic concentrations of IL-6. The reasons for these discrepancies need to be investigated in detail in the future. Nonetheless, in addition to direct blockade of IL-6

signaling, our nanoagents may exhibit a different mode of action in these mouse models, which warrants further exploration.

■ CONCLUSIONS

In summary, we developed a nanoplatform based on PdPLs to selectively deliver TCZ, an IL-6R antagonist, to the liver for site-specific targeting of IL-6R. Our data revealed that TCZ could greatly block IL-6/IL-6R signaling in our murine models. Importantly, our PdPL-PEG@TCZ nanocomplexes exhibited a much greater efficacy in ameliorating anemia than free TCZ at the same dose. Moreover, tumor growth was substantially inhibited by PdPL-PEG@TCZ administration versus TCZ treatment in the CRA model. Further mechanistic investigations revealed that our nanocomplexes may also exert antitumor effects through a different mechanism other than the direct blockade of IL-6/IL-6R signaling, involving complex intertwined direct and indirect mechanisms. These nanomedicines showed excellent biocompatibility without detectable toxicities to tissues. Thus, the potential benefits of this approach may readily be extended to other anti-inflammatory agents.

■ ASSOCIATED CONTENT

Supporting Information

The Supporting Information is available free of charge at <https://pubs.acs.org/doi/10.1021/acs.nanolett.1c04260>.

Materials and methods, histological examination of tissues from mice upon PdPL-PEG for 7 days, assessment of inflammation in mice in response to PdPL-PEG, tissue iron content and spleen changes in mice post intraperitoneal implantation of LLC cells, spleen weight changes in mice receiving LLC cell implantation with or without treatments, histological examination of tissues from mice with LLC cell implantation post different treatments, the inhibiting effect of TCZ on IL-6-stimulated proliferation in various cancer cell lines, establishment of the cancer model with inflammation but without anemia through orthotopic injection of 4T1 cells, and the therapeutic effect of PdPL-PEG@TCZ in 4T1 tumor mouse model (PDF)

■ AUTHOR INFORMATION

Corresponding Authors

Tomas Ganz – Department of Medicine, David Geffen School of Medicine, University of California, Los Angeles, California 90095, United States; Email: tganz@mednet.ucla.edu

Sijin Liu – State Key Laboratory of Environmental Chemistry and Ecotoxicology, Research Center for Eco-Environmental Sciences, Chinese Academy of Sciences, Beijing 100085, China; University of Chinese Academy of Sciences, Beijing 100049, China; orcid.org/0000-0002-5643-0734; Phone: 8610-62849330; Email: sjliu@rcees.ac.cn

Authors

Jianqiang Zhu – State Key Laboratory of Environmental Chemistry and Ecotoxicology, Research Center for Eco-Environmental Sciences, Chinese Academy of Sciences, Beijing 100085, China; Department of Urology, Tianjin Institute of Urology, The Second Hospital of Tianjin Medical University, Tianjin 300211, China

Qingfeng Fu – Department of Urology, Tianjin Institute of Urology, The Second Hospital of Tianjin Medical University, Tianjin 300211, China

Shunhao Wang – State Key Laboratory of Environmental Chemistry and Ecotoxicology, Research Center for Eco-Environmental Sciences, Chinese Academy of Sciences, Beijing 100085, China; University of Chinese Academy of Sciences, Beijing 100049, China

Liting Ren – State Key Laboratory of Environmental Chemistry and Ecotoxicology, Research Center for Eco-Environmental Sciences, Chinese Academy of Sciences, Beijing 100085, China

Wenya Feng – State Key Laboratory of Environmental Chemistry and Ecotoxicology, Research Center for Eco-Environmental Sciences, Chinese Academy of Sciences, Beijing 100085, China; University of Chinese Academy of Sciences, Beijing 100049, China

Shuting Wei – State Key Laboratory of Environmental Chemistry and Ecotoxicology, Research Center for Eco-Environmental Sciences, Chinese Academy of Sciences, Beijing 100085, China; University of Chinese Academy of Sciences, Beijing 100049, China

Zhihong Zhang – Department of Urology, Tianjin Institute of Urology, The Second Hospital of Tianjin Medical University, Tianjin 300211, China

Yong Xu – Department of Urology, Tianjin Institute of Urology, The Second Hospital of Tianjin Medical University, Tianjin 300211, China

Complete contact information is available at:

<https://pubs.acs.org/10.1021/acs.nanolett.1c04260>

Notes

The authors declare no competing financial interest.

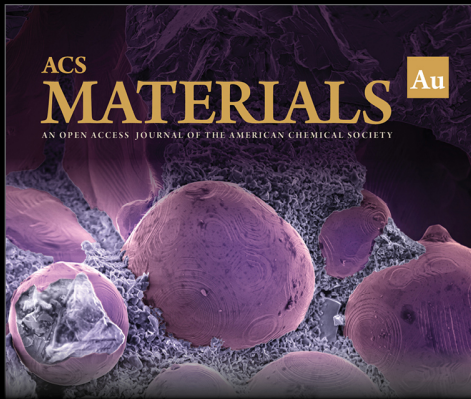
ACKNOWLEDGMENTS

This work was supported under grants from the National Natural Science Foundation of China (Grants 21920102007, 22150006, 21806123, and 22176142), the Science & Technology Development Fund of Tianjin Education Commission for Higher Education (No. 2017KJ209), Young Elite Scientists Sponsorship Program by Tianjin (No. TJSQNTJ-2020-07), and Tianjin Research Program of Application Foundation and Advanced Technology (No. 18JCQNJC80900).

REFERENCES

- (1) Birgegard, G.; Aapro, M. S.; Bokemeyer, C.; Dicato, M.; Drings, P.; Hornedo, J.; Krzakowski, M.; Ludwig, H.; Pecorelli, S.; Schmoll, H.-J.; Schneider, M.; Schrijvers, D.; Shasha, D.; van Biesen, S. Cancer-related anemia: Pathogenesis, prevalence and treatment. *Oncology-Basel* **2005**, *68*, 3–11.
- (2) Bokemeyer, C.; Oechsle, K.; Hartmann, J. T. Anaemia in cancer patients: pathophysiology, incidence and treatment. *Eur. J. Clin Invest* **2005**, *35*, 26–31.
- (3) Ludwig, H.; Van Belle, S.; Barrett-Lee, P.; Birgegard, G.; Bokemeyer, C.; Gascon, P.; Kosmidis, P.; Krzakowski, M.; Nortier, J.; Olmi, P.; Schneider, M.; Schrijvers, D. The European Cancer Anaemia Survey (ECAS): A large, multinational, prospective survey defining the prevalence, incidence, and treatment of anaemia in cancer patients. *Eur. J. Cancer* **2004**, *40* (15), 2293–2306.
- (4) Maccio, A.; Madeddu, C.; Gramignano, G.; Mulas, C.; Tanca, L.; Cherchi, M. C.; Floris, C.; Omoto, I.; Barracca, A.; Ganz, T. The role of inflammation, iron, and nutritional status in cancer-related anemia: results of a large, prospective, observational study. *Haematologica* **2015**, *100* (1), 124–32.
- (5) Abdel-Razek, H.; Hashem, H. Recent update in the pathogenesis and treatment of chemotherapy and cancer induced anemia. *Crit Rev. Oncol Hematol* **2020**, *145*, 102837.
- (6) Anand, S.; Burkenroad, A.; Glaspy, J. Workup of anemia in cancer. *Clin Adv. Hematol. Oncol* **2020**, *18* (10), 640–646.
- (7) Flint, T. R.; Fearon, D. T.; Janowitz, T. Connecting the Metabolic and Immune Responses to Cancer. *Trends Mol. Med.* **2017**, *23* (5), 451–464.
- (8) Maccio, A.; Madeddu, C.; Massa, D.; Mudu, M. C.; Lusso, M. R.; Gramignano, G.; Serpe, R.; Melis, G. B.; Mantovani, G. Hemoglobin levels correlate with interleukin-6 levels in patients with advanced untreated epithelial ovarian cancer: role of inflammation in cancer-related anemia. *Blood* **2005**, *106* (1), 362–7.
- (9) Singh, R.; Mishra, M. K.; Aggarwal, H. Inflammation, Immunity, and Cancer. *Mediators Inflamm.* **2017**, *2017*, 6027305.
- (10) Nemeth, E.; Rivera, S.; Gabayan, V.; Keller, C.; Taudorf, S.; Pedersen, B. K.; Ganz, T. IL-6 mediates hypoferrremia of inflammation by inducing the synthesis of the iron regulatory hormone hepcidin. *J. Clin Invest* **2004**, *113* (9), 1271–6.
- (11) Adamson, J. W. The anemia of inflammation/malignancy: mechanisms and management. *Hematology Am. Soc. Hematol Educ Program* **2008**, *2008*, 159–65.
- (12) Nemeth, E.; Tuttle, M. S.; Powelson, J.; Vaughn, M. B.; Donovan, A.; Ward, D. M.; Ganz, T.; Kaplan, J. Hepcidin regulates cellular iron efflux by binding to ferroportin and inducing its internalization. *Science* **2004**, *306* (5704), 2090–3.
- (13) Ganz, T. Anemia of Inflammation. *N Engl J. Med.* **2019**, *381* (12), 1148–1157.
- (14) Taniguchi, K.; Karin, M. IL-6 and related cytokines as the critical lymphins between inflammation and cancer. *Semin Immunol* **2014**, *26* (1), 54–74.
- (15) Jones, G.; Panova, E. New insights and long-term safety of tocilizumab in rheumatoid arthritis. *Ther Adv. Musculoskelet Dis* **2018**, *10* (10), 195–199.
- (16) Sebba, A. Tocilizumab: the first interleukin-6-receptor inhibitor. *Am. J. Health Syst. Pharm.* **2008**, *65* (15), 1413–8.
- (17) Mihara, M.; Kasutani, K.; Okazaki, M.; Nakamura, A.; Kawai, S.; Sugimoto, M.; Matsumoto, Y.; Ohsugi, Y. Tocilizumab inhibits signal transduction mediated by both mL-6R and sIL-6R, but not by the receptors of other members of IL-6 cytokine family. *Int. Immunopharmacol* **2005**, *5* (12), 1731–40.
- (18) Hashizume, M.; Uchiyama, Y.; Horai, N.; Tomosugi, N.; Mihara, M. Tocilizumab, a humanized anti-interleukin-6 receptor antibody, improved anemia in monkey arthritis by suppressing IL-6-induced hepcidin production. *Rheumatol Int.* **2010**, *30* (7), 917–23.
- (19) Shi, S. G.; Huang, Y. Z.; Chen, X. L.; Weng, J.; Zheng, N. F. Optimization of Surface Coating on Small Pd Nanosheets for in Vivo near-Infrared Photothermal Therapy of Tumor (vol 7, pg 14369, 2015). *ACS Appl. Mater. Inter* **2016**, *8* (45), 31482–31482.
- (20) Wu, T. S.; Tang, M. Review of the effects of manufactured nanoparticles on mammalian target organs. *J. Appl. Toxicol* **2018**, *38* (1), 25–40.
- (21) Zhang, Y. N.; Poon, W.; Tavares, A. J.; McGilvray, I. D.; Chan, W. C. W. Nanoparticle-liver interactions: Cellular uptake and hepatobiliary elimination. *J. Controlled Release* **2016**, *240*, 332–348.
- (22) Wang, S.; Li, J.; Chen, M.; Ren, L.; Feng, W.; Xu, L.; Chen, X.; Xia, T.; Zheng, N.; Liu, S. Palladium nanoplates scotch breast cancer lung metastasis by constraining epithelial-mesenchymal transition. *National Science Review* **2021**, *8* (7), nwaa226.
- (23) Chen, X. L.; Li, J. C.; Huang, Y. Z.; Wei, J. P.; Sun, D.; Zheng, N. F. The biodistribution, excretion and potential toxicity of different-sized Pd nanosheets in mice following oral and intraperitoneal administration. *Biomater Sci-Uk* **2017**, *5* (12), 2448–2455.
- (24) Rong, J.; Zhou, Z.; Wang, Y.; Han, J.; Li, C.; Zhang, W.; Ni, L. Immobilization of Horseradish Peroxidase on Multi-Armed Magnetic Graphene Oxide Composite: Improvement of Loading Amount and Catalytic Activity. *Food Technol. Biotechnol* **2019**, *57* (2), 260–271.
- (25) Tang, Y. X.; Wang, X. Y.; Li, J.; Nie, Y.; Liao, G. J.; Yu, Y.; Li, C. Overcoming the Reticuloendothelial System Barrier to Drug Delivery with a “Don’t-Eat-Us” Strategy. *ACS Nano* **2019**, *13* (11), 13015–13026.

- (26) Zhang, Y.; Cai, K.; Li, C.; Guo, Q.; Chen, Q.; He, X.; Liu, L.; Zhang, Y.; Lu, Y.; Chen, X.; Sun, T.; Huang, Y.; Cheng, J.; Jiang, C. Macrophage-Membrane-Coated Nanoparticles for Tumor-Targeted Chemotherapy. *Nano Lett.* **2018**, *18* (3), 1908–1915.
- (27) Bartucci, R.; Paramanandana, A.; Boersma, Y. L.; Olinga, P.; Salvati, A. Comparative study of nanoparticle uptake and impact in murine lung, liver and kidney tissue slices. *Nanotoxicology* **2020**, *14* (6), 847–865.
- (28) Xie, G. P.; Sun, J.; Zhong, G. R.; Shi, L. Y.; Zhang, D. W. Biodistribution and toxicity of intravenously administered silica nanoparticles in mice. *Arch. Toxicol.* **2010**, *84* (3), 183–190.
- (29) Rong, J.; Zhou, Z.; Wang, Y.; Han, J.; Li, C.; Zhang, W.; Ni, L. Immobilization of Horseradish Peroxidase on Multi-Armed Magnetic Graphene Oxide Composite: Improvement of Loading Amount and Catalytic Activity. *Food Technol. Biotechnol* **2019**, *57* (2), 260–271.
- (30) Shinohara, N.; Danno, N.; Ichinose, T.; Sasaki, T.; Fukui, H.; Honda, K.; Gamo, M. Tissue distribution and clearance of intravenously administered titanium dioxide (TiO₂) nanoparticles. *Nanotoxicology* **2014**, *8* (2), 132–141.
- (31) Liu, J.; Liu, W.; Liu, Y.; Miao, Y.; Guo, Y.; Song, H.; Wang, F.; Zhou, H.; Ganz, T.; Yan, B.; Liu, S. New thiazolidinones reduce iron overload in mouse models of hereditary hemochromatosis and beta-thalassemia. *Haematologica* **2019**, *104* (9), 1768–1781.
- (32) Johnson, D. E.; O'Keefe, R. A.; Grandis, J. R. Targeting the IL-6/JAK/STAT3 signalling axis in cancer. *Nat. Rev. Clin Oncol* **2018**, *15* (4), 234–248.
- (33) Atri, C.; Guerfali, F.; Laouini, D. Role of Human Macrophage Polarization in Inflammation during Infectious Diseases. *International Journal of Molecular Sciences* **2018**, *19* (6), 1801.
- (34) Lokau, J.; Kleinegger, F.; Garbers, Y.; Waetzig, G. H.; Grotzinger, J.; Rose-John, S.; Haybaeck, J.; Garbers, C. Tocilizumab does not block interleukin-6 (IL-6) signaling in murine cells. *PLoS One* **2020**, *15* (5), No. e0232612.
- (35) Liu, J.; Sun, B. B.; Yin, H. J.; Liu, S. J. Hepcidin: A Promising Therapeutic Target for Iron Disorders A Systematic Review. *Medicine* **2016**, *95* (14), e3150.
- (36) Hou, Y. L.; Zhang, S. P.; Wang, L.; Li, J. P.; Qu, G. B.; He, J. Y.; Rong, H. Q.; Ji, H.; Liu, S. J. Estrogen regulates iron homeostasis through governing hepatic hepcidin expression via an estrogen response element. *Gene* **2012**, *511* (2), 398–403.
- (37) Lee, S. O.; Yang, X.; Duan, S.; Tsai, Y.; Strojny, L. R.; Keng, P.; Chen, Y. IL-6 promotes growth and epithelial-mesenchymal transition of CD133+ cells of non-small cell lung cancer. *Oncotarget* **2016**, *7* (6), 6626–38.
- (38) Liu, Y.; Qi, Y.; Yin, C.; Wang, S.; Zhang, S.; Xu, A.; Chen, W.; Liu, S. Bio-transformation of Graphene Oxide in Lung Fluids Significantly Enhances Its Photothermal Efficacy. *Nanotheranostics* **2018**, *2* (3), 222–232.
- (39) Wang, S.; Shao, J.; Li, Z.; Ren, Q.; Yu, X. F.; Liu, S. Black Phosphorus-Based Multimodal Nanoagent: Showing Targeted Combinatory Therapeutics against Cancer Metastasis. *Nano Lett.* **2019**, *19* (8), 5587–5594.
- (40) Yin, C. Y.; Wang, S. H.; Ren, Q. Z.; Shen, X. M.; Chen, X. D.; Liu, Y. J.; Liu, S. J. Radial extracorporeal shock wave promotes the enhanced permeability and retention effect to reinforce cancer nanothermotherapeutics. *Sci. Bull.* **2019**, *64* (10), 679–689.
- (41) Johnson, D. E.; O'Keefe, R. A.; Grandis, J. R. Targeting the IL-6/JAK/STAT3 signalling axis in cancer. *Nat. Rev. Clin Oncol* **2018**, *15* (4), 234–248.
- (42) Kim, A.; Fung, E.; Parikh, S. G.; Valore, E. V.; Gabayan, V.; Nemeth, E.; Ganz, T. A mouse model of anemia of inflammation: complex pathogenesis with partial dependence on hepcidin. *Blood* **2014**, *123* (8), 1129–1136.
- (43) Goumas, F. A.; Holmer, R.; Egberts, J. H.; Gontarewicz, A.; Heneweer, C.; Geisen, U.; Hauser, C.; Mende, M. M.; Legler, K.; Rocken, C.; Becker, T.; Waetzig, G. H.; Rose-John, S.; Kalthoff, H. Inhibition of IL-6 signaling significantly reduces primary tumor growth and recurrences in orthotopic xenograft models of pancreatic cancer. *Int. J. Cancer* **2015**, *137* (5), 1035–46.
- (44) Orabona, C.; Mondanelli, G.; Pallotta, M. T.; Carvalho, A.; Albini, E.; Fallarino, F.; Vacca, C.; Volpi, C.; Belladonna, M. L.; Berlioli, M. G.; Ceccarini, G.; Esposito, S. M.; Scattoni, R.; Verrotti, A.; Ferretti, A.; De Giorgi, G.; Toni, S.; Cappa, M.; Matteoli, M. C.; Bianchi, R.; Matino, D.; Iacono, A.; Puccetti, M.; Cunha, C.; Bicciato, S.; Antognelli, C.; Talesa, V. N.; Chatenoud, L.; Fuchs, D.; Pilotte, L.; Van den Eynde, B.; Lemos, M. C.; Romani, L.; Puccetti, P.; Grohmann, U. Deficiency of immunoregulatory indoleamine 2,3-dioxygenase 1 in juvenile diabetes. *JCI Insight* **2018**, *3* (6), e96244.
- (45) Wu, R.; Liu, X.; Yin, J.; Wu, H.; Cai, X.; Wang, N.; Qian, Y.; Wang, F. IL-6 receptor blockade ameliorates diabetic nephropathy via inhibiting inflammasome in mice. *Metabolism* **2018**, *83*, 18–24.
- (46) Ueda, O.; Tateishi, H.; Higuchi, Y.; Fujii, E.; Kato, A.; Kawase, Y.; Wada, N. A.; Tachibe, T.; Kakefuda, M.; Goto, C.; Kawaharada, M.; Shimaoka, S.; Hattori, K.; Jishage, K. Novel genetically-humanized mouse model established to evaluate efficacy of therapeutic agents to human interleukin-6 receptor. *Sci. Rep* **2013**, *3*, 1196.



ACS
MATERIALS Au
AN OPEN ACCESS JOURNAL OF THE AMERICAN CHEMICAL SOCIETY

Editor-in-Chief: **Prof. Shelley D. Minteer**, University of Utah, USA

Deputy Editor:
Prof. Stephanie L. Brock
Wayne State University, USA

Open for Submissions 

pubs.acs.org/materialsau  ACS Publications
Most Trusted. Most Cited. Most Read.